HAL open science

Rational formulation design of injectable thermosensitive chitosan-based hydrogels for cell encapsulation and delivery

Phuong Anh Dang, Carla Palomino-Durand, Mohamed Elsafi Mabrouk, Pierre Marquaille, Clément Odier, Sophie Norvez, Emmanuel Pauthe, Laurent Corté

▶ **To cite this version:**

Phuong Anh Dang, Carla Palomino-Durand, Mohamed Elsafi Mabrouk, Pierre Marquaille, Clément Odier, et al.. Rational formulation design of injectable thermosensitive chitosan-based hydrogels for cell encapsulation and delivery. Carbohydrate Polymers, 2021, pp.118836. 10.1016/j.carbpol.2021.118836 . hal-03420627

HAL Id: hal-03420627

https://hal.science/hal-03420627v1

Submitted on 5 Jan 2024

HAL is a multi-disciplinary open access archive for the deposit and dissemination of scientific research documents, whether they are published or not. The documents may come from teaching and research institutions in France or abroad, or from public or private research centers.

L'archive ouverte pluridisciplinaire **HAL**, est destinée au dépôt et à la diffusion de documents scientifiques de niveau recherche, publiés ou non, émanant des établissements d'enseignement et de recherche français ou étrangers, des laboratoires publics ou privés.

Distributed under a Creative Commons Attribution - NonCommercial 4.0 International License

Version of Record: https://www.sciencedirect.com/science/article/pii/S0144861721012236
Manuscript_ed36bd9df0e5d08a7bbe8439b33f437e

Rational formulation design of injectable thermosensitive chitosan-based hydrogels for cell encapsulation and delivery

Phuong Anh Dang[1,2], Carla Palomino-Durand[2], Mohamed Elsafi Mabrouk[1], Pierre Marquaille[1], Clément Odier[1], Sophie Norvez[1], Emmanuel Pauthe[2], Laurent Corté [1,3].*

[1] Molecular, Macromolecular and Materials, C3M, ESPCI Paris, CNRS, PSL University, 10 rue Vauquelin, 75005, Paris, France.

[2] Équipe de Recherche sur les Relations Matrice Extracellulaire-Cellule, ERRMECe, CY Cergy Paris Université, Maison Internationale de la Recherche, 1 rue Descartes, 95000, Neuville-sur-Oise, France.

[3] Centre des Matériaux, MINES ParisTech, CNRS, PSL University, 63-65 rue Henri-Auguste Desbruères, 91003, Evry, France.

© 2021 published by Elsevier. This manuscript is made available under the CC BY NC user license
https://creativecommons.org/licenses/by-nc/4.0/

ABSTRACT (150 words)

This work reports a rational design of injectable thermosensitive chitosan systems for cell encapsulation and delivery. Using mixtures of two phosphate salts, beta-glycerophosphate and ammonium hydrogen phosphate, we demonstrate that the pH and the osmolarity can be adjusted separately by varying the molar ratios between the salts and the D-glucosamine monomers. We found the existence of a critical temperature above which gelation time decays following a power-law. This gelation kinetics can be finely tuned through the pH and salt-glucosamine ratios. Formulations having physiological pH and osmolarity were produced for chitosan concentrations ranging from 0.4 to 0.9 wt%. They remain liquid for more than 2 h at 20°C and form a macroporous gel within 2 min at 37°C. *In vitro* encapsulation of pre-osteoblastic cells and gingival fibroblasts showed homogeneous cell distribution and good cell viability up to 24 h. Such an approach provides a valuable platform to design thermosensitive cell-laden systems.

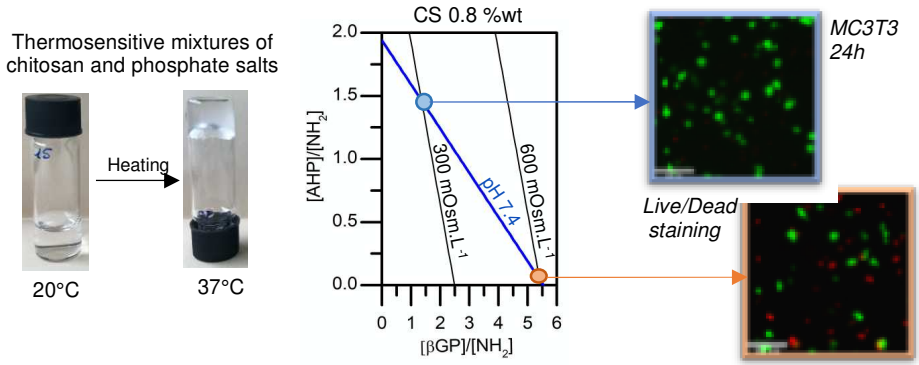

KEYWORDS: thermosensitive hydrogel, chitosan, phosphate salt, injectable vehicle, cell encapsulation, cell delivery

INTRODUCTION

Cell-laden injectable hydrogels have raised a great interest during the last decades as valuable delivery vehicles or matrices for cell therapies (Li, Rodrigues, & Tomás, 2012). Administrated in a minimally invasive manner, these gels fill-in the defects in hardly accessible and fragile tissues, and might provide a temporary scaffold to injected cells to ensure their viability and stimulate their activity. For effective clinical applications, such systems should stay liquid before and during injection, then gel rapidly in physiological conditions for temperature, pH and osmolarity. In the liquid state, pH and osmolarity should be finely controlled for the survival of the encapsulated cells. After gelation, the gel scaffold must provide appropriate mechanical and chemical properties as well as a macroporosity enabling cell invasion and growth. Different stimuli-responsive systems for *in situ* gelling have been investigated, triggered by temperature (Yap & Yang, 2020), pH (Z. Li et al., 2016), or light (Neves et al., 2017). Among those, thermogelling hydrogels based on biocompatible chitosan have been extensively studied (Mekhail & Tabrizian, 2014).

Chitosan (CS) is a linear copolymer composed of D-glucosamine and N-acetyl-D-glucosamine monomers (**Figure 1**). CS is obtained by alkaline deacetylation of parent chitin, a primary component of cell walls in fungi and crustacean shells. As one of the few representatives of biodegradable and biocompatible polymers approved for clinical use (Berger et al., 2004; Riva et al., 2011; Saravanan, Vimalraj, Thanikaivelan, Banudevi, & Manivasagam, 2019) CS has long been a popular biomaterial for developing cell delivery matrices (Di Martino, Sittinger, & Risbud, 2005; Zhou, Jiang, Cao, Li, & Chen, 2015). Amino groups of chitosan present an apparent pKa_{app} in the vicinity of 6.2. At pH < pKa_{app}, CS behaves as a cationic polyelectrolyte bearing protonated amino groups, soluble in aqueous media. Near neutral pHs where CS is

mostly deprotonated, the strong tendency of the carbohydrate polymer to self-associate through H-bonding and hydrophobic interactions dominates, giving rise to the formation of a hydrated gel-like precipitate (Rinaudo, 2006). This poor solubility of CS at physiological pHs has long been a major limitation for biomedical uses, until the pioneering work by Chenite et al., who demonstrated that in presence of beta-glycerophosphate (βGP, **Figure 1**), cationic CS solutions turned into thermally sensitive solutions, remaining liquid at room temperature even at neutral pHs, and forming hydrogels around 37°C (Chenite et al., 2000, 2001).

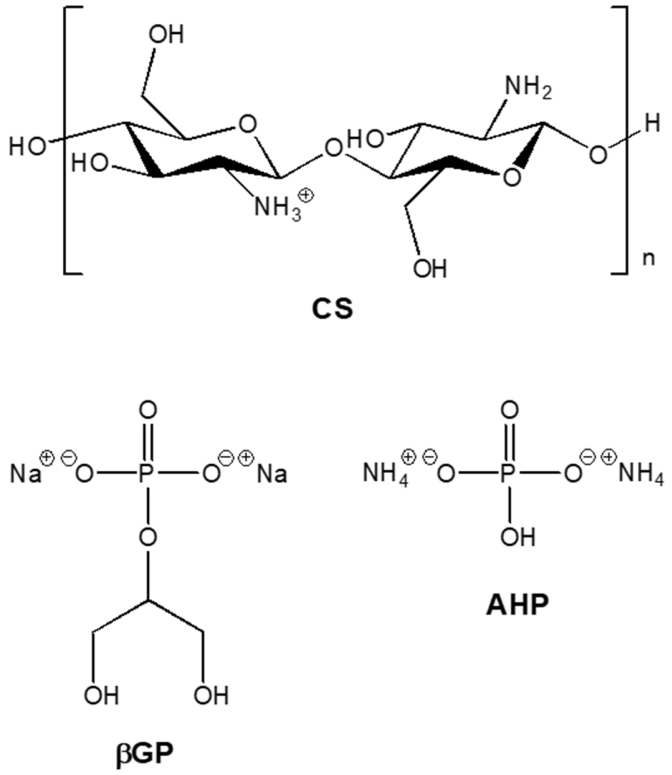

Figure 1. Structures of chitosan CS, β-glycerophosphate βGP and ammonium hydrogen phosphate AHP.

The mechanisms responsible for the thermoresponsivity of CS-βGP mixtures are still debated. Cho et al. associated the gelling mechanism with enhanced hydrophobic interactions with increasing temperatures (Cho, Heuzey, Bégin, & Carreau, 2005, 2006). Filion et al. underlined

that the pKa_{app} of CS decreases by heating, producing a release of protons that may be accepted by the negatively charged βGP, a weak base having a $pK_{a,2}$ of 6.65 at 25°C. The CS neutralization induced by the temperature-dependent proton transfer would result in a phase separation of the chitosan solution (Filion, Lavertu, & Buschmann, 2013; Lavertu, Filion, & Buschmann, 2008). Thermodynamic insights into the mechanism of the phase transition of CS induced by βGP have been recently related by Grinberg et al. (2020). From calorimetric analyses, they concluded that the βGP binding induces the formation of a highly ordered hydrate structure of the polysaccharide, causing a large entropic stress despite the stability brought by stabilization of the complexes. Heating thus leads to dehydration and release of βGP ligands, accompanied by a transfer of protons from CS to βGP due to the simultaneous decrease in the ionization constant of CS as already suggested by Lavertu, Filion, & Buschmann (2008). By losing their charges and hydrated structures, CS chains eventually tend to self-associate and form a gel.

These CS-βGP mixtures appeared clearly as a promising thermo-gelling system for cell injection, remaining liquid at physiological pH and turning rapidly into a gel at body temperature. However, increasing salt concentrations to reach appropriate values of pH also increases the osmolarity of the mixture up to cytotoxic values (Ahmadi & De Bruijn, 2008). Hence, strategies were implemented to improve the standard system, mostly by replacing partially or totally βGP by other salts. Using ammonium hydrogen phosphate (AHP, **Figure 1**), a lower salt concentration was required to reach neutral pHs (7.0 – 7.2) resulting in physiological osmolarity (300 ± 30 $mOsm.L^{-1}$) (Nair, Starnes, Ko, & Laurencin, 2007). Other inorganic phosphate salts without polyol moieties, like dipotassium hydrogen phosphate K_2HPO_4 (Ta, Han, Larson, Dass, & Dunstan, 2009), basic sodium phosphates as NaH_2PO_4, Na_2HPO_4, or even Na_3PO_4 (X. Y. Li et al., 2010; Casettari, Cespi, Palmieri, & Bonacucina, 2013), have also been studied to produce

90 thermo-sensitive CS formulations. Sodium hydrogen carbonate (SHC) has been studied as a
91 gelling agent, alone (Huang, Yu, Feng, & Li, 2011; Liu, Tang, Wang, & Guo, 2011) or in
92 combination with βGP (Assaad, Maire, & Lerouge, 2015; Ceccaldi et al., 2017; Deng, Kang,
93 Zhang, Yang, & Yang, 2017; Alinejad, Adoungotchodo, Hui, Zehtabi, & Lerouge, 2018).
94 Mixtures of CS/AHP (Nair, Starnes, Ko, & Laurencin, 2007) or CS/βGP/SHC (Ceccaldi et al.,
95 2017 ; Alinejad, Adoungotchodo, Hui, Zehtabi, & Lerouge, 2018) have been evaluated *in vitro* as
96 3D scaffolds for cells. Encapsulation of mouse preosteoblastic cells and fibroblasts as well as
97 human mesenchymal stem cells confirmed the cytocompatibility for days for some formulations.
98 The feasibility of using these chitosan-based hydrogels as a cell carrier vehicle has therefore been
99 demonstrated. Nevertheless, the numerous variables, pH, osmolarity, salt and chitosan
100 concentrations leading to injectable cytocompatible solutions are all interdependent. A general
101 platform is still lacking, enabling to control independently pH and osmolarity, and therefore
102 gelation kinetics and cytocompatibility, whatever the chitosan concentration. Yet, controlling
103 chitosan concentration is a key to adjust the viscoelastic and microstructural properties of the
104 injected hydrogels, which are of the utmost importance to favor cell anchorage and growth.

105 In this study we present a rational formulation design to make thermosensitive CS solutions, by
106 partially replacing βGP by AHP in the mixture. With this third component, AHP, we can
107 decouple the control on pH and osmolarity, whatever the CS concentration. We show that these
108 two parameters can be adjusted independently by the simple ratios [salt]/[NH_2], where [NH_2]
109 denotes the concentration in D-glucosamine monomer in the solution, *i.e.* the concentration in
110 deacetylated chitin monomers bearing NH_2 functions. This approach gives rise to a robust
111 platform, to easily formulate physiological solutions able to form a gel within a couple of minutes
112 at body temperature. We investigated in depth the gelation kinetics for physiological formulations

113 and determined a critical temperature of gelation, under which the system remains liquid
114 overtime, for different CS concentrations. We checked the cytocompatibility of our controlled
115 CS/βGP/AHP formulations and explored the effect of osmolarity on cell activity by
116 encapsulating preosteoblastic mouse cells (MC3T3-E1) and human gingival fibroblasts (HGF).
117 By means of confocal microscopy and rheology, we showed that hydrogel microstructure and
118 mechanical properties can be varied by changing CS concentration while maintaining fixed pH
119 and osmolarity.

120 **EXPERIMENTAL METHODS**

121 **1. Materials & Cells**

122 Three grades of chitosan (CS) having high purity (impurity level < 1.0%) were purchased from
123 Glentham Life Sciences Limited. All the study was performed with chitosan low molar mass
124 (viscosity 30-100 cps) having the following characteristics given by the supplier: deacetylation
125 degree DD = 91%, as measured by potentiometric titration, average molar mass M_w = 250
126 $kg.mol^{-1}$, as measured by viscosimetry. For pH titration experiments, two other grades with DD
127 of 95 % were also used: chitosan very low molar mass (10 cps) with M_w = 30 $kg.mol^{-1}$, and
128 chitosan (100-300 cps) with M_w = 890 $kg.mol^{-1}$.
129 β-glycerophosphate disodium salt hydrate BioUltra (βGP) and ammonium hydrogen phosphate
130 BioUltra (AHP) were purchased from Sigma-Aldrich. Glacial acetic acid (AcOH, 99%) was
131 purchased from Alfa Aesar. Alexa Fluor 488 was purchased from Abcam. The Live/Dead™ kit
132 and AlamarBlue™ reagent were purchased from Invitrogen. MC3T3-E1 pre-osteoblastic cells
133 were procured from ATCC®, and human gingival fibroblasts were isolated from healthy donors
134 and kindly donated by Laboratory BioS, Reims University. α–MEM, DMEM, phosphate buffer
135 saline without calcium and magnesium (PBS) were purchased from Gibco. Deionized distilled
136 water from a Milli-Q system was used to prepare all aqueous solutions.
137

138 **2. Methods**

139 *2.1.Preparation and sterilization of reactants*

140 Aqueous suspensions of CS were sterilized in autoclave at 121°C for 10 min using standard
141 liquid cycle according to San Juan et al. (2012). After autoclaving, acetic acid (AcOH) was added

142 to the suspension with molar ratio [AcOH]/[NH_2] = 1, which was stirred at room temperature
143 (21±1°C) for 24 h. The concentration of the CS stock solution was 1.33 wt%. CS stock solutions
144 were stored at 5°C until further use. βGP, AHP and AcOH solutions at 1 mol.L^{-1} were prepared
145 in deionized water and sterilized by filtration using syringe filters having pore size of 0.2 µm.

146 2.2. *pH titration of CS/βGP solution with AHP solution*

147 Stock solutions of βGP and AHP as well as CS solution at 0.8 wt% were chilled in an ice bath
148 prior to mixture. All pH titrations were performed at 4 ± 1°C. The βGP solution was added
149 dropwise to the CS solution under vigorous stirring. Solutions with molar ratio [βGP]/[NH_2]
150 ranging from 0 to 4 were prepared. For each [βGP]/[NH_2] ratio, titration was carried out with
151 AHP solution until the pH reached 7.4.

152 *2.3. Osmolarity measurement*

153 Osmolality of different solutions was measured with a cryoscopic osmometer (Osmomat 30,
154 Gonotec). The apparatus measures the osmolality (mOsm.kg^{-1}), which is proportional through
155 the density to the osmolarity (mOsm.L^{-1}). In this study, since all solutions are diluted, the
156 difference between osmolarity and osmolality is insignificant.

157 *2.4. Gelation time measurement*

158 The gelation times were determined by the test tube inversion method. The sol phase was defined
159 as the flowing phase and the gel phase as the non-flowing phase when the test tube was inverted.
160 1 mL of CS/βGP solutions was introduced into 1.5 mL tubes that were incubated in a thermostat
161 at fixed temperature (15-37°C). Time between inversions was as follows: 30 s from 0 to 10 min,
162 1 min from 10 to 30 min, 5 min from 30 to 60 min, 10 min from 60 to 120 min, 15 min from 2 h

163 to 5 h, 30 min from 5 h to 10 h and 3 h after 10 h. The time at which the gel did not flow anymore
164 was recorded as the gelation time and the time interval between two inversions gave the
165 experimental uncertainty. Each measure was duplicated. The shortest measurable gelation time is
166 given by the duration of thermal equilibration, which in these tubes was measured to be 1 min for
167 a solution at 4°C immersed in a thermostat at 37°C.

168 *2.5. Microstructure study of CS/βGP/AHP hydrogels*

169 CS was labelled with Alexa Fluor 488 (Alexa Fluor monomer units:NH_2 = 1:150) following a
170 protocol adapted from Zhang et al. (2011). The fluorescently labelled CS was then added to
171 regular CS suspensions before the autoclave process. Labelled CS chains represented only 0.5
172 wt% of the total amount of CS in each formulation. The amount of grafted fluorophore was three
173 orders of magnitude smaller than in Zhang et al. (AlexaFluor/NH_2 units 1:30000). Hence, the
174 perturbation caused by the labelling was considered to be negligible. Accordingly, there was no
175 difference in gelation time at 37°C between regular CS and fluorescently labelled CS.

176 A sample holder was filled with a few hundreds of microliters of fluorescently labelled
177 CS/βGP/AHP solution, sealed to prevent evaporation and incubated in a regular oven at 37°C for
178 30 min. Hydrogels at CS concentrations between 0.5 and 0.8 wt% were observed at room
179 temperature using Laser Confocal Scanning Microscopy (LCSM, Zeiss Axiovert 200M). For
180 each sample, stacks of 10 images of (225 µm x 225 µm) with an interval of 1 µm were recorded
181 in eight random positions at 100 µm depth.

182 Deconvolution of the image stacks was performed using the Iterative Deconvolve 3D plugin with
183 a theoretical point spread function PSF calculated by the Diffraction PSF 3D plugin (ImageJ).
184 Deconvoluted images were binarized using Li's method (C. H. Li & Tam, 1998). The polymer-

185 rich zones are presented in white and the polymer-poor zones (pores) are presented in black. The
186 porosity was determined as the percentage of black pixels over the total number of pixels. The
187 pore size distribution was characterized quantitatively using a customized algorithm (Python)
188 based on the morphological sieve technique (Wu, van Vliet, Frijlink, & van der Voort
189 Maarschalk, 2007). This technique calculates on each image the fraction of porosity that is able to
190 fit a structuring element having a given shape and size, here a disk having a given diameter. For
191 each formulation, the average porosity and average pore size distribution were calculated over 8
192 stacks of 10 images.

193 *2.6. Rheological characterization*

194 Rheological properties of physiological formulations prepared with 0.5 wt% or 0.8 wt% of CS
195 were studied using rheometer MCR502 (Anton Paar) with a cone-and-plate geometry (CP50-
196 2TG). The temperature was managed by a Peltier controller and the geometry was previously
197 stabilized at 18°C. Formulations were loaded immediately after preparation and silicone oil was
198 added to the interface between the sample and the air to prevent evaporation.

199 For isothermal measurement, the temperature was rapidly increased 37°C at a rate of 20°C.min^{-1}.
200 The values of storage and loss moduli (G', G") were measured during 6 h, at a constant
201 oscillatory strain of 0.1% and an angular frequency of 1 rad.s^{-1}. For temperature sweep
202 measurement, the temperature was increased from 4°C to 60°C then decreased from 60°C to 4°C,
203 at a rate of 5°C/min. The values of storage and loss moduli (G', G") were measured during one
204 heating/cooling cycle, at a constant oscillatory strain of 0.1% and an angular frequency of 1 rad.s^{-}
205 ^{1}.

206 *2.7. Injectability evaluation*

207 Injectability test was performed using the protocol reported by Kondziolka, Gobbel, Fellows-
208 Mayle, Chang, & Uram (2011). For visualization, a small amount of rose Bengal dye was added
209 to CS/βGP/AHP mixture. Immediately following the preparation, the mixture was loaded into a 5
210 mL syringe equipped with a 21G needle and placed on a pump syringe. A volume of 1.5 mL was
211 then injected at a rate of 250 $\mu L.min^{-1}$ into a PBS solution at pH 7.4 and 37°C.

212 *2.8. Cell encapsulation in thermosensitive chitosan hydrogels*

213 We compared two formulations of hydrogels for cell encapsulation: CS/βGP (600 $mOsm.L^{1}$) and
214 CS/βGP/AHP (300 $mOsm.L^{-1}$) at fixed CS concentration (0.8 wt%) and at pH 7.4 on two cell
215 models: primary human gingival fibroblast (HGF) and pre-osteoblast immortalized murine cell
216 line (MC3T3-E1). HGF were cultured in DMEM and MC3T3-E1 cells were cultured in
217 α–MEM, both cell culture medium supplemented with 10%v/v fetal calf serum and 1%v/v
218 penicillin-streptomycin. For both cell types, the encapsulation protocol was as follows: (1) cells
219 were trypsinized and mixed gently with CS/βGP or CS/βGP/AHP solutions at a final
220 concentration of 10^6 $cells.mL^{-1}$; (2) 300 μL of the mixture containing cells were dispensed into a
221 24-well culture plate (Nunc™ F96 MicroWell™) and incubated for 1 h at 37°C and 5% CO_2 to
222 induce gelation; (3) 1 mL of culture medium supplemented with 10%v/v fetal calf serum and
223 1%v/v penicillin-streptomycin was added into each well. Hydrogels without cells were also
224 prepared by replacing the cell suspension by culture medium.

225 *2.9. Live/Dead assay*

226 After 1 h or 24 h, the encapsulated cells were stained using calcein AM/ethidium homodimer
227 (CalAM/EthD-1) mixture at optimized concentrations ([CalAM]/[EthD-1]: 2 μM/2 μM and 1

228 μM/0.5 μM for MC3T3-E1 cells and HGF, respectively). For positive control, cells were seeded
229 directly into the well at a density of 10^4 cells.cm^{-2}. For negative control, cells were killed using
230 methanol solution at 70 wt%. 1 mL of the staining mixture was added into each well and the
231 plates were incubated at 37°C and 5% CO_2 for 45 min then the mixture was removed and the
232 hydrogels or cells were rinsed with PBS. 500 μL of PBS solution were added into each well to
233 prevent drying. The distribution and the state of the cells were visualized using a laser scanning
234 confocal microscope (LSM 710, Zeiss) using lasers at 488 nm and 561 nm. Each hydrogel sample
235 was scanned from bottom to 300 μm depth at 8 random positions. Stacks were taken at 20x
236 magnification and a 512x512 pixel resolution with the pinhole at 1 Airy unit and interval of 4
237 μm. Recorded images were then analyzed with ImageJ using 3D Object counter plugin (Bolte &
238 Cordelières, 2006). The cell viability (%) was determined as the number of living cells over the
239 total number of cells. Experiments were carried out with n = 2 for MC3T3 and n = 1 for HGF and
240 all samples were prepared in triplicate.

241 *2.10. AlamarBlue assay*

242 The cell metabolism was evaluated using the AlamarBlue assay at 1 h and 24 h following
243 encapsulation. After incubation, a solution of 10 %v/v AlamarBlue in culture medium (1
244 mL/well) was added directly on each hydrogel and incubated for 3 h at 37°C and 5 % of CO_2.
245 Then, the supernatant was homogenized by pipetting and 150 μL were transferred into a 96-well
246 plate (Nunc™ F96 MicroWell™). The intensity of fluorescence was determined by using Xenius
247 XM spectrofluorometer (SAFAS Monaco) at 560 nm excitation and 590 nm emission. A value of
248 the metabolic activity per cell was estimated by normalizing the measured intensity by the
249 number of living cells obtained from the Live/Dead assay.

250 *2.11. Statistical analysis*

251 Statistical analysis was performed using a t-test with normality assumption. Statistical
252 significance was accepted at the level of $p < 0.05$.

253 **RESULTS & DISCUSSION**

254 In all the following, [NH_2] denotes the concentration in D-glucosamine monomer in the solution.

255 **1. Controlling the pH using CS/βGP/AHP formulations**

256 Control of the pH of thermogelling CS/βGP solutions is determinant for the viability and the
257 injectability of encapsulated cells. Cell viability requires that the pH be maintained close to 7.4
258 during cell suspension and storage until injection and immersion in other buffering media. The
259 gelation time of CS/βGP solutions was also shown to depend greatly on pH (Chenite et al., 2001).
260 Accordingly, we measured that the gelation time of CS/βGP solutions increases from 1 min to
261 10 h when pH decreases from 7.5 to 7.1 (**Figure S1**). In the present study, CS was dissolved in
262 acidic aqueous solutions with a fixed molar ratio [AcOH]/[NH_2] = 1. This ratio was chosen as the
263 minimum amount of acid required to ensure the solubilization of chitosan chains (Rinaudo,
264 2006). In CS/βGP/AHP formulations, βGP and AHP are both weak bases that raise the pH of the
265 solution. As demonstrated thereafter, the pH can be finely controlled by the molar ratios between
266 each phosphate salt and D-glucosamine monomer, [βGP]/[NH_2] and [AHP]/[NH_2].

267 We carried out pH titration at 4°C by adding AHP (1 mol.L^{-1}) to solutions having an initial CS
268 concentration of 0.8 wt% and different ratios of [βGP]/[NH_2]. The evolution of pH as a function
269 of [AHP]/[NH_2] is reported in **Figure 2a**. For a given [βGP]/[NH_2], all titration curves show an
270 increase in pH with increasing [AHP]/[NH_2]. Similarly, for a given [AHP]/[NH_2], pH increases
271 with increasing [βGP]/[NH_2]. From those curves, we extracted the pairs of ratios [βGP]/[NH_2]
272 and [AHP]/[NH_2] producing a given pH and built the iso-pH curves represented in **Figure 2b**.
273 Those iso-pH curves are linear in the studied range of pH from 7.0 to 7.4. Formulations using the

274 ratios of the iso-pH curve at 7.4 but different initial CS concentrations (0.5 and 0.6 wt%) exhibit
275 a pH 7.4 as well, which confirms that the pH is fully determined by the ratios [βGP]/[NH_2] and
276 [AHP]/[NH_2], irrespectively of the CS concentrations.

277 The pH of CS and CS/βGP solutions is known to decrease substantially with increasing
278 temperature (Lavertu et al., 2008; Supper et al., 2013). A similar effect was observed in the
279 CS/βGP/AHP formulations. For instance, the pH of a solution at CS 0.8 wt% decreases from 7.40
280 ± 0.05 at 4°C to 6.95 ± 0.05 at 37°C (**Figure S2**). Therefore, it seems more appropriate to target
281 formulations having a pH 7.4 at 4°C to ensure that the pH of cell-laden solutions remains within a
282 physiological range (typically 7.0-7.4) during cell dispersion and encapsulation.
283

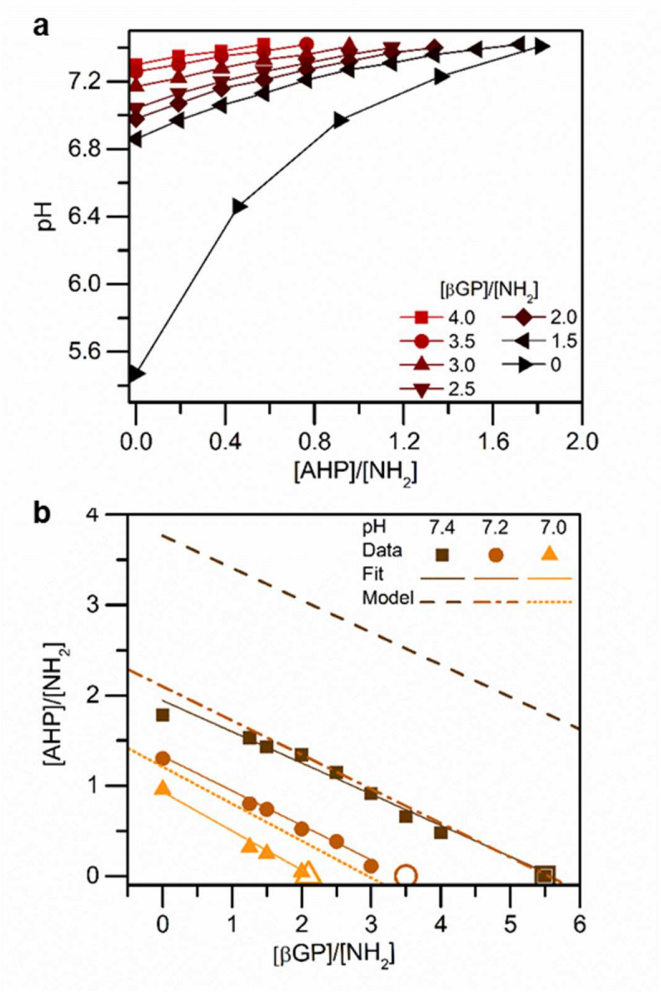

284

285 **Figure 2.** (**a**) Evolution of the pH as a function of [AHP]/[NH_2] for formulations with initial CS
286 concentration of 0.8 wt% and [βGP]/[NH_2] ranging from 0 to 4. (**b**) Iso-pH curves at 7.0, 7.2 and 7.4 as a
287 function of [AHP]/[NH_2] and [βGP]/[NH_2]. Experimental data are shown as filled symbols. Linear fitting
288 curves are shown as continuous lines and model predictions as interrupted lines. Predictions accounting
289 for the polyelectrolyte effect based on Filion et al., 2007 are shown as open symbols for CS/βGP mixtures
290 ([AHP]/[NH_2] = 0).

291 The linear relationship observed in **Figure 2b** can be rationalized by considering the dissociation
292 of the different species present in the solution, as follows:

293 $$NH_3^+ \rightleftharpoons NH_2 + H^+ \text{ , } K_{CS} \quad (1)$$

$$AcOH \rightleftharpoons AcO^- + H^+ \text{ , } K_{Ac} \quad (2)$$

$$AHP \rightleftharpoons AHP^- + H^+ \rightleftharpoons AHP^{2-} + 2H^+ \text{ , } K_{AHP,1} \text{ \& } K_{AHP,2} \quad (3)$$

$$\beta GP \rightleftharpoons \beta GP^- + H^+ \rightleftharpoons \beta GP^{2-} + 2H^+ \text{ , } K_{\beta GP,1} \text{ \& } K_{\beta GP,2} \quad (4)$$

$$H_2O \rightleftharpoons H^+ + OH^- \quad (5)$$

The values of the dissociation constants of AHP and βGP were measured by pH titration at 4°C and 25°C (**Figure S3**). Only the second equilibrium is observed for pH ranging from 2 to 8: $K_{AHP,2} = 10^{-6.7}$ and $K_{\beta GP,2} = 10^{-6.2}$. For CS and AcOH, values are chosen from the literature: $K_{CS} = 10^{-7.1}$ (4°C) (Filion et al., 2013) and $K_{Ac} = 10^{-4.8}$ (Kortum, Vogel, & Andrussow, 1960).

To a first approximation, we assume here that CS behaves like a small molecule and we do not take into account its polyelectrolyte nature. Writing electroneutrality, conservation of matter and acid-base equilibria, we find that for the pH range of interest (7.0-7.4), the ratios $[AHP]/[NH_2]$ and $[\beta GP]/[NH_2]$ satisfy the following relation (see detailed calculation in SI):

$$\frac{[AHP]}{[NH_2]} = -\frac{C_{\beta GP}}{C_{AHP}} \cdot \frac{[\beta GP]}{[NH_2]} + \frac{C_{Ac}}{C_{AHP}} \cdot \frac{[AcOH]}{[NH_2]} - \frac{C_{CS}}{C_{AHP}.DD} \quad (6)$$

where $[AcOH], [\beta GP], [AHP], [NH_2]$ are respectively the initial concentrations in AcOH, βGP, AHP and D-glucosamine monomer, DD is the degree of deacetylation of CS. Factors C_{Ac}, $C_{\beta GP}$, C_{AHP} and C_{CS} are all functions of the concentration in protons h as follows: $C_{Ac} = \left(1 + \frac{h}{K_{Ac}}\right)^{-1}$, $C_{\beta GP} = \left(1 + \frac{K_{\beta GP,2}}{h}\right)^{-1}$, $C_{AHP} = \left(1 + \frac{K_{AHP,2}}{h}\right)^{-1}$ and $C_{CS} = \left(1 + \frac{K_{CS}}{h}\right)^{-1}$.

For a fixed ratio $[AcOH]/[NH_2]$, here equal to 1, equation (6) captures that for a given pH, the relationship between $[AHP]/[NH_2]$ and $[\beta GP]/[NH_2]$ is linear. The negative slope $-\frac{C_{\beta GP}}{C_{AHP}}$ depends

weakly on the pH of the mixture and the dissociation constants of the two salts βGP and AHP. The model predicts the experimental values of the slopes with a good precision including the slight increase when the pH decreases from 7.4 to 7.0, as shown in **Figure 2b** and **Table S1**. However, it fails to predict the intercept. We attribute this discrepancy to the polyelectrolyte nature of CS. In particular, the protonation of NH_2 along the CS chains is very sensitive to entropic effects and pK_{CS} increases with increasing salt concentration (Filion et al., 2007). Accordingly, predictions of pH for CS/βGP accounting for these polyelectrolyte effects using a model by Filion et al. (**Figure S4**) are in perfect agreement with our experimental measurements, as indicated by the open symbols in **Figure 2b**. The simple small molecule model also confirms that the linear relationship between [AHP]/[NH_2] and [βGP]/[NH_2] is independent on the CS concentration as long as the ratio [AcOH]/[NH_2] is fixed. Therefore, such iso-pH curves may serve as an efficient platform to prepare CS/βGP/AHP formulations having a controlled pH.

2. CS/βGP/AHP formulations with adjustable pH and osmolarity

The contribution of βGP, AHP and AcOH to the osmolarity of the formulations was determined by measuring independently their osmolarity at different concentrations. We verified that osmolarity was proportional to the molar concentration for all three components (**Figure S5**). As expected from the dissociation constants, the osmolarity induced by βGP is higher than the one induced by AHP. The osmolarity of a CS solution at 0.8 wt% is negligible. The total osmolarity (expressed in $Osm.L^{-1}$) was calculated as the linear combination of the three contributions:

$$\text{Osmolarity} = 1.03\cdot[\text{AcOH}] + 2.35\cdot[\beta\text{GP}] + 1.82\cdot[\text{AHP}] \quad (7)$$

Normalizing Equation (7) by [NH_2] gives a relationship between [AHP]/[NH_2] and [βGP]/[NH_2]:

334 $$\frac{[\mathrm{AHP}]}{[\mathrm{NH_2}]} = -\mathrm{A_1}.\frac{[\beta\mathrm{GP}]}{[\mathrm{NH_2}]} - \mathrm{A_2}.\frac{[\mathrm{AcOH}]}{[\mathrm{NH_2}]} + \mathrm{A_3}.\frac{\mathrm{Osmolarity}}{[\mathrm{NH_2}]} \quad (8)$$

335 where $A_1 = 1.29$, $A_2 = 0.57$ and $A_3 = 0.55$ are dimensionless constants.

336 For a fixed ratio [AcOH]/[NH_2], we obtain linear iso-osmolarity lines between [AHP]/[NH_2] and
337 [βGP]/[NH_2]. Unlike the iso-pH curves above, the intercept of these curves depends on the CS
338 concentration. The curves obtained for a physiological osmolarity of 300 mOsm.L^{-1} are presented
339 in **Figure 3a** for CS concentrations ranging from 0.4 to 1.2 wt%. For a given CS concentration,
340 the intersection between the iso-pH (pH = 7.4) and iso-osmolarity lines give the unique
341 formulation satisfying both conditions on targeted pH and osmolarity.

342 The representation in **Figure 3a** provides a way to determine the formulations of interest for
343 thermosensitive cell-laden hydrogels. In particular, it shows that the double constraint on pH and
344 osmolarity restricts the range of pertinent CS concentrations. As shown in **Figure 3a**, CS
345 concentration of 0.4 wt% is the lowest concentration allowing to achieve physiological pH (7.4)
346 and osmolarity (300 mOsm.L^{-1}). CS concentrations lower than 0.4 wt% would require either a
347 hypotonic mixture to satisfy pH = 7.4 or a basic pH (>7.4) to satisfy an osmolarity of 300
348 mOsm.L^{-1}. We verified that the physiological formulation at 0.4 wt% corresponding to
349 [βGP]/[NH_2] = 5.5 and [AHP]/[NH_2] = 0 forms a macroscopically homogeneous gel after 2 min
350 at 37°C (**Figure 3b**). In **Figure 3a**, the highest CS concentration allowing to achieve
351 physiological pH and osmolarity is 1.2 wt%. However, this concentration (corresponding to
352 [βGP]/[NH_2] = 0) is not pertinent for practical applications, because the gelation time at room
353 temperature (i.e. before injection) decreases when decreasing [βGP]/[NH_2], as will be presented
354 in section 3. We found that a minimum ratio [βGP]/[NH_2] = 1.0, corresponding to a CS
355 concentration of 0.9 wt%, is required to maintain the thermosensitive solution in a liquid state for

356 more than 1 h at 21±1°C. A duration of 1 h corresponds to the time needed to comfortably carry
357 out cell trypsination, dispersion in CS/salt solution and injection. Accordingly, solutions prepared
358 at a higher concentration than 0.9 wt% form a gel in less than 1 h at room temperature, as shown
359 for example for a 1 wt% solution ([βGP]/[NH_2] = 0.7, [AHP]/[NH_2] = 1.7) which formed a gel
360 within 30 min (**Figure 3c**).

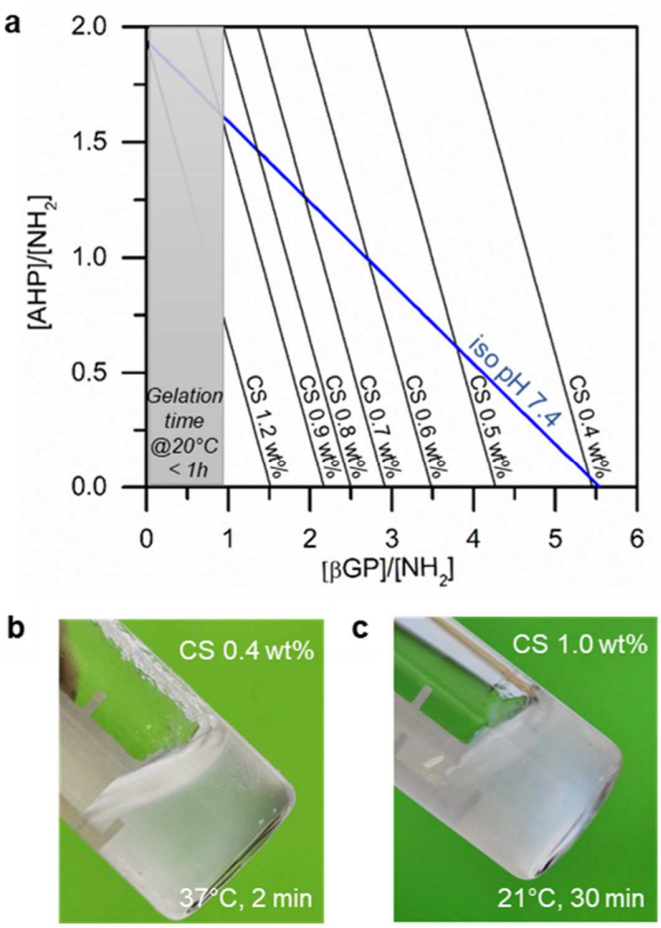

361

362 **Figure 3.** (**a**) Iso-osmolarity curves at 300 mOsm.L^{-1} (black) and iso-pH curve at 7.4 (blue) as a function
363 of [AHP]/[NH_2] and [βGP]/[NH_2] for CS concentration ranging from 0.4 to 1.2 wt%. Shaded area
364 indicates formulations for which gelation time at 21°C is less than 1 h. (**b**) Hydrogel (300 mOsm.L^{-1}; pH =
365 7.4) obtained with 0.4 wt% of CS after 2 min of incubation at 37°C, (**c**) Hydrogel (300 mOsm.L^{-1}; pH =
366 7.4) obtained with 1.0 wt% of CS after 30 min at 21±1°C.

367 These results and methodology show how the pH and osmolarity of CS/βGP/AHP mixtures can
368 be independently adjusted for different CS concentrations. It is worth to note that the
369 concentration range for cytocompatible values of pH and osmolarity has been measured here for
370 one type of CS having a given degree of deacetylation (DD = 91 %) and a given molar mass
371 distribution (viscosity 30-100 cps, Mw = 250 kg.mol^{-1}). It has been reported that the gelation rate
372 of CS/βGP solutions at given pH increases with CS of higher DD (Ruel-Gariépy, Chenite,
373 Chaput, Guirguis, & Leroux, 2000). Therefore, the upper bound of the accessible concentration
374 range is expected to decrease with increasing DD. As regards the molar mass, we verified that the
375 pH can be adjusted by the salts/NH_2 ratios whatever the chitosan chain length is as long as the
376 deacetylation degree is known, as shown for CS with DD = 95 % for two different molar masses
377 (**Figure 4**). Hence, this rationalized formulation is applicable to other types of CS.

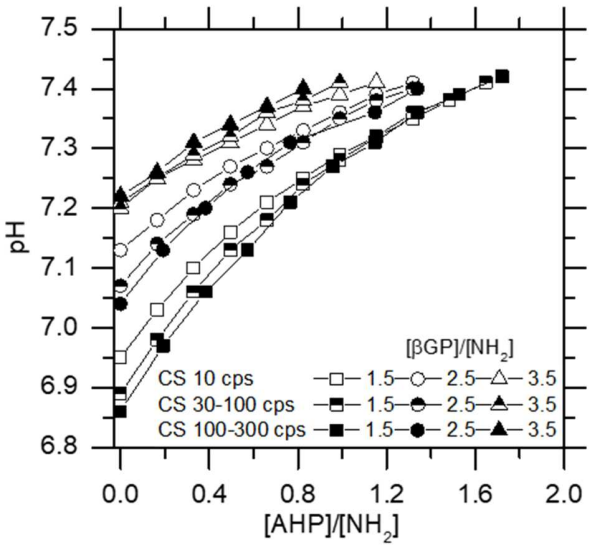

378

379 **Figure 4.** Evolution of the pH as a function of [AHP]/[NH_2] in formulations with initial CS concentration
380 of 0.8 wt% and fixed [βGP]/[NH_2] = 1.5, 2.5 and 3.5 for three different chitosan grades (10 cps, 30-100
381 cps and 100-300 cps) having DD = 95%, 91% and 95%, respectively.

382 **3. Gelation kinetics of CS/βGP/AHP formulations**

383 It is important to notice that the gelation time of CS/βGP systems depends greatly on the pH
384 (Chenite et al., 2001). As a result, we focus here on the gelation kinetics at a fixed pH = 7.4.
385 **Figure 5** shows the evolution of storage, G', and loss modulus, G", during a heating-cooling cycle
386 between 4 and 60°C for CS/βGP and CS/βGP/AHP, both at pH 7.4. While heating, both moduli
387 exhibit a sharp increase and the gel point (G' = G") is reached near 45°C for CS/βGP and 40°C
388 for CS/βGP/AHP. Upon cooling, a large hysteresis is observed and both moduli decrease slowly
389 below 30°C. This weak thermoreversibility is very similar to what has been reported earlier by
390 Chenite et al. (2001).

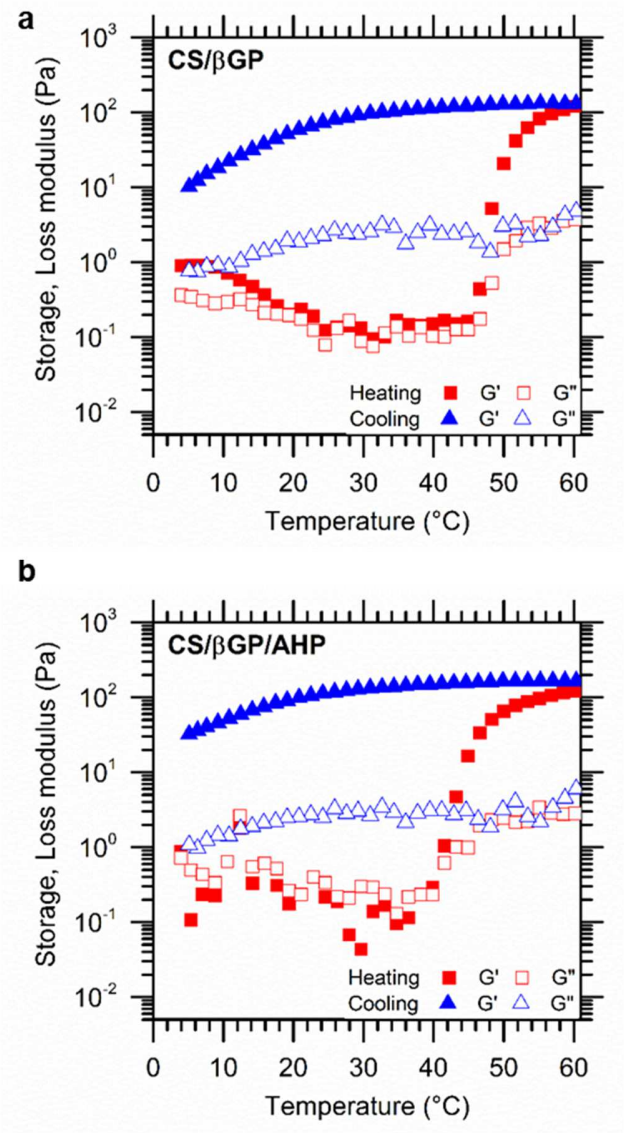

Figure 5. Evolution of the storage and loss modulus during a heating/cooling cycle for CS/βGP mixture (a) and CS/βGP/AHP mixture (b), both at fixed pH of 7.4, CS concentration of 0.8 wt%.

A more systematic characterization of the thermosensitivity of CS/βGP/AHP mixtures was performed using the test tube inversion method (**Figure S6a**). We verified that the time measured by this method is consistent with the time to reach the gel point as determined by rheology (**Figure S6b-c**). In a first series of experiments, we studied the effect of the relative salt ratio [AHP]/[βGP] on the gelation time. For that, a fixed CS concentration of 0.8 wt% was chosen.

399 Four ratios [βGP]/[NH_2] were studied (0, 1.5, 3 and 5.5) and the corresponding [AHP]/[NH_2]
400 ratios were adjusted to maintain pH = 7.4 (1.9, 1.4, 0.8 and 0, respectively). In those solutions,
401 the osmolarity varied from 300 to 600 mOsm.L^{-1}. **Figure 6a** shows that the gelation time
402 decreases by at least four orders of magnitude when temperature increases from 15°C to 37°C for
403 all four formulations. At a given temperature, the gelation time decreases with decreasing
404 [βGP]/[NH_2] ratio or increasing [AHP]/[NH_2] ratio. This sensitivity to [AHP]/[βGP] becomes
405 increasingly pronounced with decreasing temperature. At 20°C, the formulation with only βGP
406 become a gel more than 100 times slower than the one with AHP only.

407 The temperature dependence of the gelation time of CS/βGP formulations was presented in an
408 earlier study by Chenite et al. (2001) who concluded that the gelation time displayed an
409 exponential decay with temperature. Our data which cover a larger range of times and
410 temperatures do not fit with a simple exponential decay, but rather with a model of critical
411 transition, as already observed in thermosensitive gelatin gels (Te Nijenhuis, 1979). Our
412 experimental data were successfully fitted with the critical-like model $t_{gel} = k(T-T_c)^{\gamma}$ where T_c is
413 a critical temperature above which the sol-gel transition occurs and γ is a critical exponent
414 (**Figure 6b**). The exponent γ and the prefactor k decrease with increasing [βGP]/[NH_2] (**Figure**
415 **S7a-b**). Conversely, T_c increases from 4 to 18°C when going from CS/AHP to CS/βGP as shown
416 in **Figure 6c**. Overall these results show that the thermal stability of CS/βGP/AHP solutions at a
417 fixed pH increases with [βGP]/[NH_2]. This observation together with the rheological results in
418 Figure 5 supports the hypothesis that the polyol part of βGP hinders the interactions between CS
419 chains as suggested by Supper et al. (2013).

420 Similar experiments were performed in a second series with formulations defined by the iso-pH
421 (7.4) and iso-osmolarity (300 mOsm.L^{-1}) curves for different CS concentrations ranging from 0.5
422 to 0.8 wt%. The gelation time decayed strongly with increasing temperature in a similar way to
423 the first series, as shown in **Figure 6d**. For a given temperature, gelation occurred faster with
424 increasing CS concentration (together with decreasing [βGP]/[NH_2] and increasing [AHP]/[NH_2]
425 to maintain physiological conditions). Again, a critical power law behavior was observed as
426 shown in **Figure 6e** (and **Figure S7c-d**). The critical temperature, and therefore the thermal
427 stability of the solution, decreased with increasing CS concentration.

428 From a practical point of view, these results show that all the formulations having physiological
429 pH and osmolarity present an adequate gelation kinetics for use as cell delivery vehicles. At
430 21°C, they remain liquid for more than 2 h, which is appropriate for cell dispersion and
431 manipulation. At body temperature, they form a gel within less than 1 min, therefore preventing
432 cells from being dispersed away. The injectability of the formulation having a CS concentration
433 of 0.8 wt% was verified using standard injection parameters into a PBS solution at 37°C. A
434 continuous injection could be performed with the quasi-instantaneous formation of a macroscopic
435 hydrogel (**Video S1**).

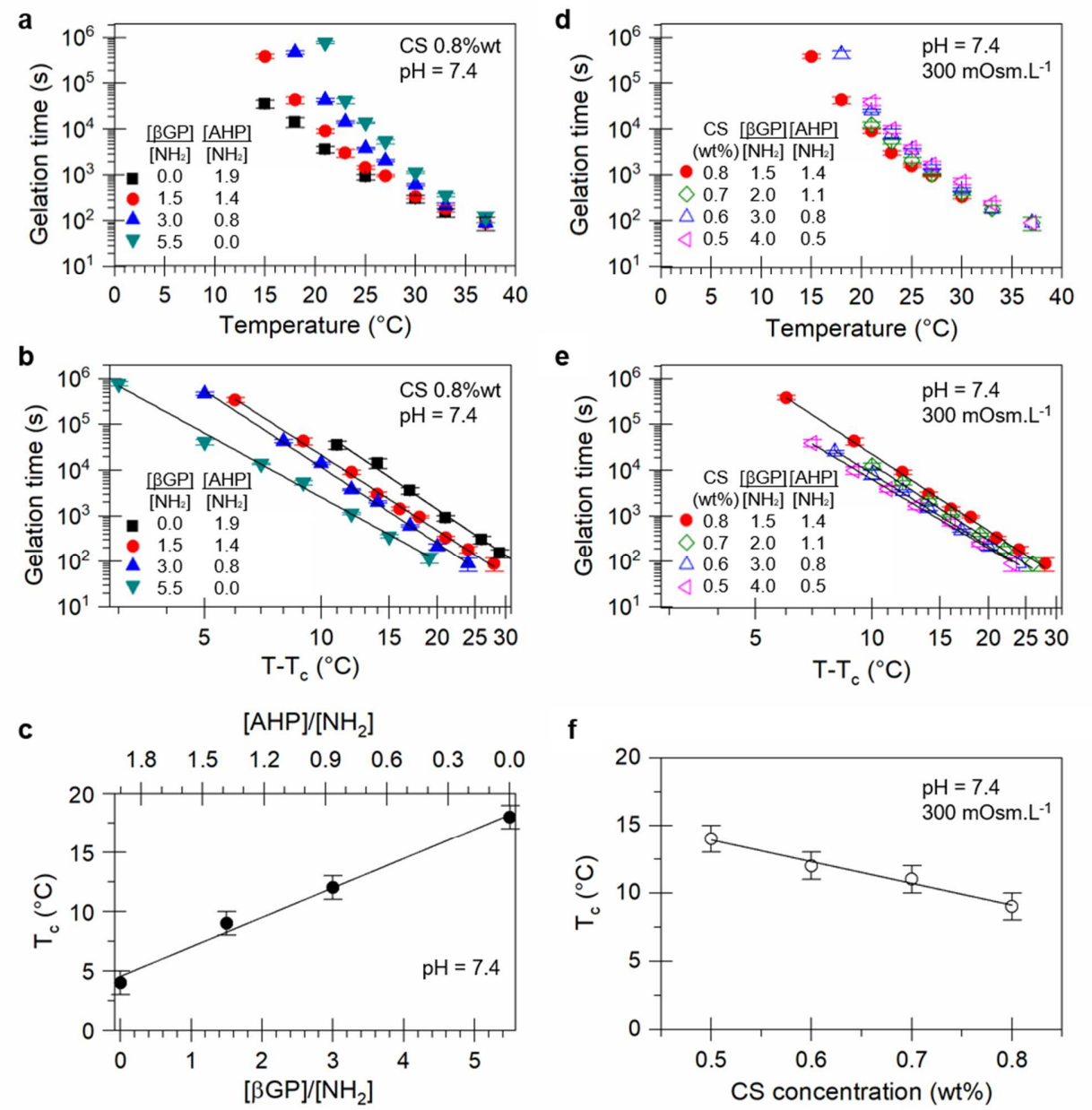

Figure 6. (**a-c**) Gelation kinetics of formulations having fixed CS 0.8 wt% and pH 7.4 and various [βGP]/[NH_2] and [AHP]/[NH_2] ratios. Gelation time as a function of temperature (**a**) and (T-T_c) (**b**). Full lines show fits by a power law. (**c**) Critical temperature as a function of [βGP]/[NH_2] and [AHP]/[NH_2]. (**d-f**) Gelation kinetics of physiological formulations (pH = 7.4 and 300 mOsm.L^{-1}) for CS concentration ranging from 0.5 to 0.8 wt%. Gelation time as a function of temperature (**d**) and (T-T_c) (**e**). Full lines show fits by a power law. (**f**) Critical temperature as a function of CS concentration.

443 **4. Cell encapsulation in CS/βGP/AHP hydrogels**

444 The viability and the metabolism of encapsulated cells was studied using Live/Dead and
445 AlamarBlue assays with formulations having a CS concentration of 0.8 wt% and pH 7.4. Two
446 formulations were compared to assess the effect of osmolarity: an isotonic formulation denoted
447 CS/βGP/AHP (300 mOsm.L^{1}) produced with ratios [βGP]/[NH_2] = 1.5 and [AHP]/[NH_2] = 1.4,
448 and a hypertonic formulation denoted CS/βGP (600 mOsm.L^{-1}) obtained with ratios [βGP]/[NH_2]
449 = 5.5 and [AHP]/[NH_2] = 0. Two cell types were studied: pre-osteoblast immortalized murine cell
450 line (MC3T3-E1) and primary human gingival fibroblasts (HGF). Cells were dispersed in the
451 liquid formulations at 20°C at a concentration of 10^6 cells. mL^{-1}. Encapsulation was achieved by
452 gelation at 37°C for 1 h in an incubator prior to the addition of culture medium. Cells were
453 stained and observed 1 h and 24 h after encapsulation. The staining efficiency was verified on
454 positive and negative controls (**Figure S8**). The homogeneity of the cell dispersion was verified
455 by cell counting in multiple areas of the gels (**Figure S9**) and a local cell concentration of 1.2 x
456 10^6 ± 0.2 cells per cm^3 was found, which is in agreement with the density of seeded cells.

457 Typical images obtained with Live/Dead staining are shown in **Figure 7a-b** for MC3T3-E1 and
458 HGF, respectively. At 1 h, the viability for both cell types is high (90%) for the two studied
459 formulations (**Figure 7c**). At 24 h, differences are observed: for MC3T3-E1 cells, a significantly
460 better cell viability is observed in CS/βGP/AHP hydrogel (78 ± 6 %) than in CS/βGP hydrogel
461 (52 ± 5 %); for HGF, cell viability remains high in both hydrogels. The metabolic activity of the
462 encapsulated cells was assessed with an AlamarBlue assay (**Figure 7d**). A value of the metabolic
463 activity per cell was estimated by normalizing the measured intensity by the number of living
464 cells. At 1 h, a clear difference can be seen between the two cell types: MC3T3 have a much

465 higher metabolic activity in the isotonic formulation CS/βGP/AHP than in CS/βGP while HGF
466 have a similar metabolic activity in both formulations. At 24 h, the same trend is observed but the
467 metabolic activity drops significantly for both cell types.

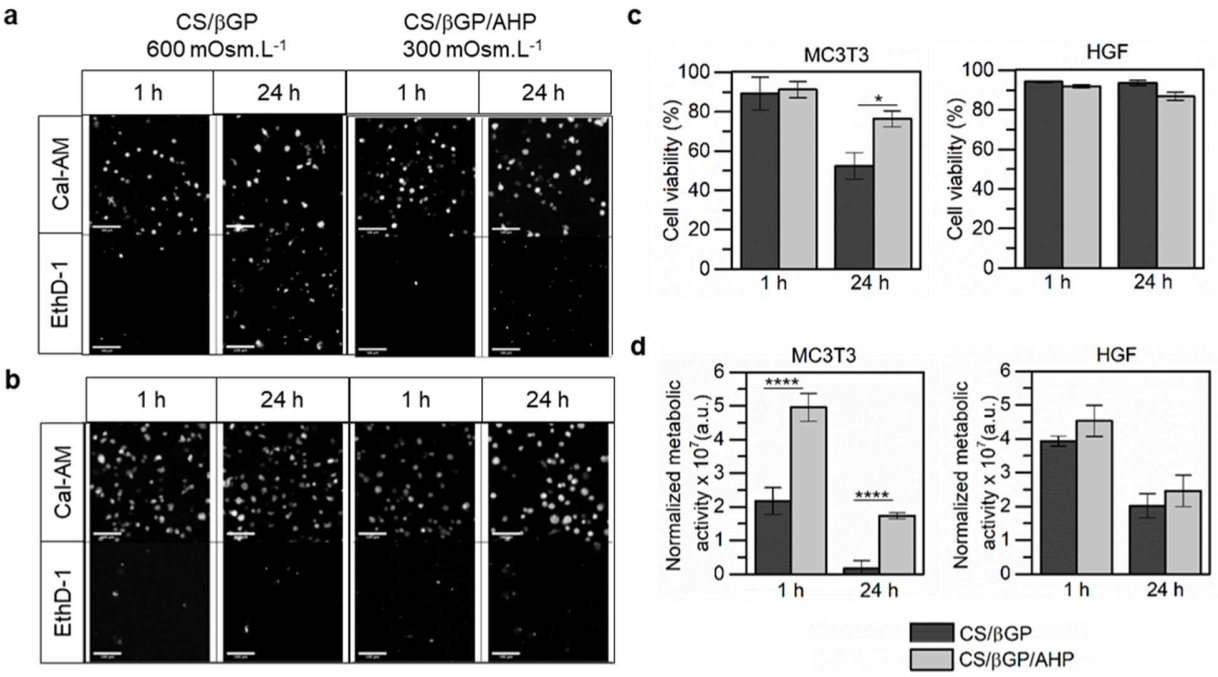

468

469 **Figure 7**. Cell encapsulation in CS/βGP/AHP and CS/βGP hydrogels for 1 h and 24 h. (**a-b**) Confocal
470 images of Live/Dead assays for MC3T3 (**a**) and HGF (**b**) cells. Images are obtained from the projection of
471 76 slices taken at a random position in the hydrogel with a field of 425 x 425 x 300 µm. (**c**) Cell viability.
472 (**d**) Normalized metabolic activity. Statistically significant at $p < 0.05$ (*) or $p < 0.0001$ (****).

473

474 These differences in viability and activity may be explained by the different ability of the cell
475 types to adapt to hypertonic conditions (Dmitrieva & Burg, 2005). To our knowledge, no study
476 has been reported on MC3T3-E1 whereas it has been shown that HGF are resistant to osmotic
477 shocks (Huynh, Everts, Leethanakul, Pavasant, & Ampornaramveth, 2016). In our study, the
478 encapsulated cells exhibit rounded phenotypes after 24 h, which reflects a poor adhesion to the
479 chitosan matrix. This observation is in agreement with a previous study on encapsulated MC3T3-

480 E1 in CS/AHP hydrogels (Nair et al., 2007). Therefore, the proposed approach could be
481 advantageously combined with bio-functionalization strategies providing adhesion sites to the
482 encapsulated cells. For example, covalent grafting of peptides or proteins responsible for cell
483 adhesion on chitosan chains have shown promising results (Custodio, Alves, Reis, & Mano,
484 2010; Tsai, Chen, & Liu, 2013).

485 **5. Microstructure and mechanics of CS/βGP/AHP hydrogels**

486 The possibility to vary the CS concentration while maintaining physiological conditions, provides
487 a way to adjust the microstructure and the mechanical properties of cytocompatible formulations.
488 The microstructure of hydrogels (pH = 7.4 and 300 $mOsm.L^{-1}$) was characterized by LSCM using
489 fluorescently labelled formulations. After 30 min at 37 °C, heterogeneous structures were
490 observed composed of interconnected polymer-rich and polymer-poor phases, the latter being
491 qualified as pores (**a**). We measured that the porosity (%) decreases linearly with increasing CS
492 concentration as shown in **Figure 8b**, from 75 ± 5 % for CS 0.5 wt% to 63 ± 7 % for CS 0.8 wt%.
493 Such a linear relationship was reported earlier for CS/βGP (Crompton et al., 2006). Besides
494 porosity, the pore size is a crucial parameter governing cell-cell interactions and vascularization
495 (Kaivosoja et al., 2012). Targeted pore sizes vary from tens to hundreds of micrometers
496 depending on the cell type and on the application (Kaivosoja et al., 2012; O'Brien, Harley,
497 Yannas, & Gibson, 2005). With the present systems, we observed large interconnected elongated
498 macropores. The longest dimension of the largest pores was found to reach 15 μm for CS 0.8
499 wt% and up to 30 μm for CS 0.5 wt%. Pore size distribution was analyzed quantitatively by
500 image analysis using a morphological sieve algorithm. The distributions in **Figure 8c** show the
501 fraction of porosity able to fit a circular structuring element of a given diameter. This analysis

clearly reveals that the characteristic size of the macropores increases with decreasing CS concentration. Indeed, 98% of the porosity can contain structuring elements having diameters ranging from 1 to 9 µm for CS 0.8 wt% and from 1 to 14 µm for CS 0.5 wt%.

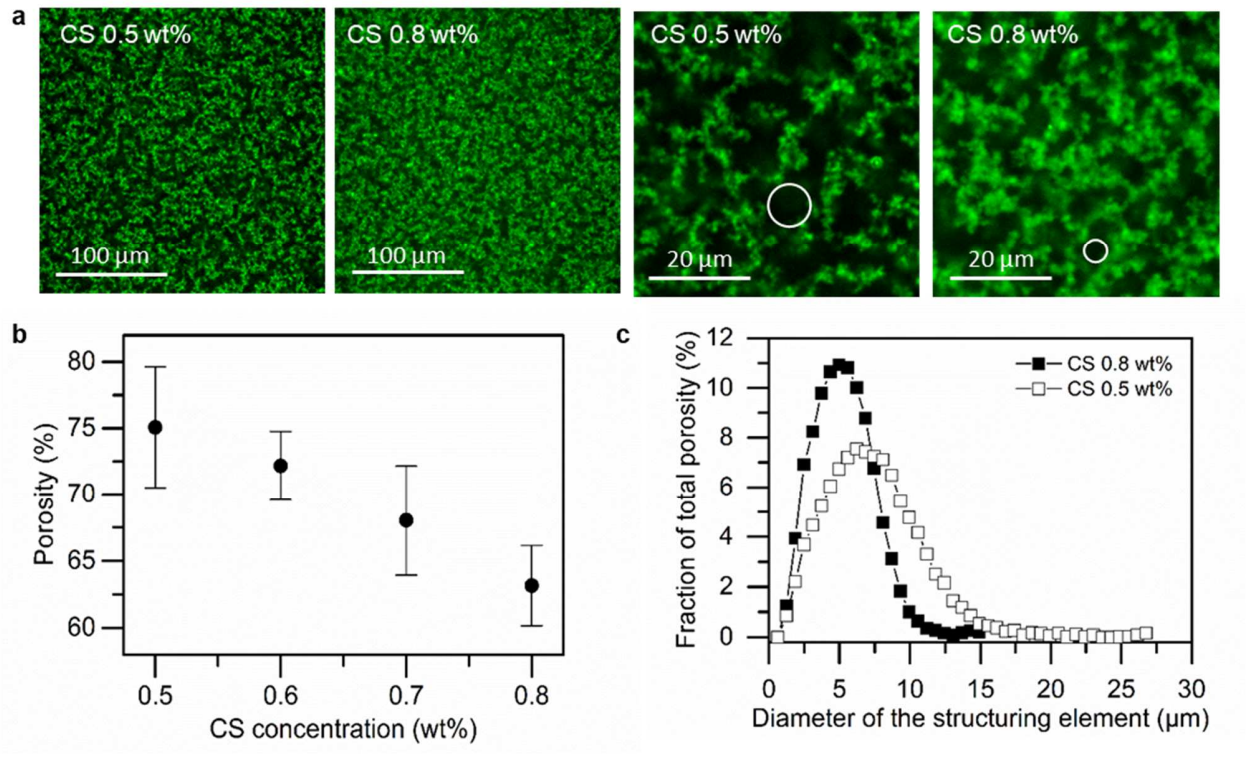

Figure 8. (**a**) Confocal images of fluorescently labelled CS/βGP/AHP hydrogels prepared with 0.5 or 0.8 wt% after 30 min at 37°C, white circles show circular structuring elements having the mean diameter determined by a morphological sieve algorithm. (**b**) Hydrogel porosity as a function of CS concentration. (**c**) Pore size distributions determined by morphological sieve technique for CS/βGP/AHP hydrogels prepared with 0.5 and 0.8 wt%.

The mechanical properties of hydrogels prepared with 0.5 and 0.8 wt% at 4°C were characterized by oscillatory rheology during an isotherm at 37°C as shown in **Figure 9**. Gelation occurs within one minute for both formulations with a rapid increase in the storage modulus (G') reaching approximately 30 Pa for 0.5 wt% and 180 Pa for 0.8 wt% at 1 h of incubation. After 6 h, G'

515 reaches 60 Pa for 0.5 wt% and 300 Pa for 0.8 wt%. These values of G' are low as compared to
516 the ones of most biological tissues. For this reason, these hydrogels might be more particularly
517 appropriate for very soft tissues, such as brain tissue which G' is in the range 100-300 Pa (Tabet
518 et al., 2019). Accordingly, CS gels were shown to be suitable matrices for cells of the nervous
519 system (Kornev, Grebenik, Solovieva, Dmitriev, & Timashev, 2018).

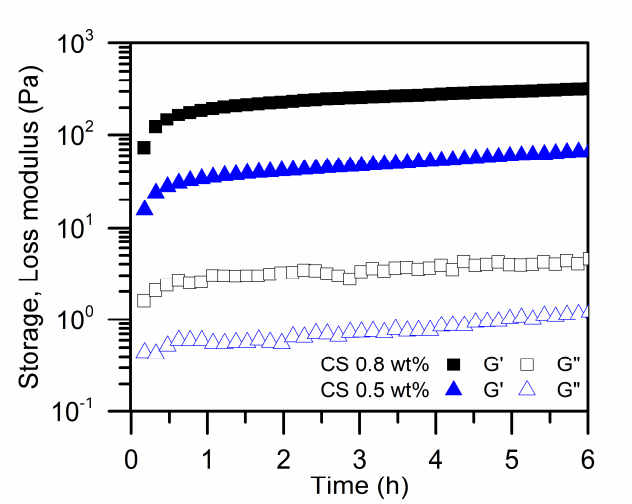

520

521 **Figure 9**. Storage modulus (G') and loss modulus (G") as function of time at 37°C for physiological
522 formulations prepared with a CS concentration of 0.5 wt% ([βGP]/[NH_2] = 4.0 and [AHP]/[NH_2] = 0.5)
523 and 0.8 wt% ([βGP]/[NH_2] = 1.5 and [AHP]/[NH_2] = 1.4).

524 **CONCLUSION**

525 In this study, we report a rational formulation design to prepare thermo-gelling systems
526 composed of chitosan CS and two phosphate salts, βGP and AHP. We show how the pH and the
527 osmolarity can be adjusted independently by the ratios [salts]/[NH_2], arising possibility to obtain
528 physiological formulations having tunable CS concentration. Moreover, a systematic study of the
529 gelation kinetics revealed that the gelation time follows a power law that diverges at a critical
530 temperature. With this approach, injectable solutions having a pH of 7.4 and a physiological
531 osmolarity of 300 $mOsm.L^{-1}$ can be produced for CS concentrations ranging from 0.4 to 0.9 wt%.
532 The cytocompability of the subsequent gels was demonstrated by *in vitro* encapsulation of
533 MC3T3-E1 and HGF cells. Elastic moduli of the gels can reach up to 300 Pa, a value found in
534 brain tissues. The proposed methodology could be applied to solutions of chitosan or
535 functionalized chitosan having various molar mass and deacetylation degrees, therefore providing
536 a general platform to prepare valuable thermosensitive hydrogels for cell encapsulation and
537 delivery.

538

539 **ACKNOWLEDGMENTS**

540 We thank Louison Blivet for technical support on the study of M_w effect, Michel Cloître and
541 Mickael Pomes-Hadda (C3M, ESPCI Paris-PSL) for their help and advice on rheology, Jean
542 Baudry and Florence Condamine (CBI, ESPCI Paris-PSL) for their help on osmometry, Lamia El
543 Guermah and Remy Agniel (ERRMECe, CYU) for technical support on the cell culture and
544 characterization. We thank Etienne Decencière (CMM, MINES ParisTech-PSL) for his help and
545 advice on image analysis. We thank the Laboratory BioS, Reims University for their donation of

546 HGF cells. Financial support from the Région Île-de-France (DIM Respore) is gratefully
547 acknowledged.

548 **REFERENCES**

549 Ahmadi, R., & De Bruijn, J. D. (2008). Biocompatibility and gelation of chitosan-glycerol phosphate hydrogels.
550 *Journal of Biomedical Materials Research - Part A*, *86*(3), 824–832. https://doi.org/10.1002/jbm.a.31676

551 Assaad, E., Maire, M., & Lerouge, S. (2015). Injectable thermosensitive chitosan hydrogels with controlled gelation
552 kinetics and enhanced mechanical resistance. *Carbohydrate Polymers*, *130*, 87–96.
553 https://doi.org/10.1016/j.carbpol.2015.04.063

554 Berger, J., Reist, M., Mayer, J. M., Felt, O., Peppas, N. A., & Gurny, R. (2004). Structure and interactions in
555 covalently and ionically crosslinked chitosan hydrogels for biomedical applications. *European Journal of*
556 *Pharmaceutics and Biopharmaceutics*, *57*(1), 19–34. https://doi.org/10.1016/S0939-6411(03)00161-9

557 Bolte, S., & Cordelières, F. P. (2006). A guided tour into subcellular colocalization analysis in light microscopy.
558 *Journal of Microscopy*, *224*(3), 213–232. https://doi.org/10.1111/j.1365-2818.2006.01706.x

559 Casettari, L., Cespi, M., Palmieri, G. F., & Bonacucina, G. (2013). Characterization of the interaction between
560 chitosan and inorganic sodium phosphates by means of rheological and optical microscopy studies.
561 *Carbohydrate Polymers*, *91*(2), 597–602. https://doi.org/10.1016/j.carbpol.2012.08.037

562 Ceccaldi, C., Assaad, E., Hui, E., Buccionyte, M., Adoungotchodo, A., & Lerouge, S. (2017). Optimization of
563 Injectable Thermosensitive Scaffolds with Enhanced Mechanical Properties for Cell Therapy. *Macromolecular*
564 *Bioscience*, *17*(6), 1–10. https://doi.org/10.1002/mabi.201600435

565 Chenite, A., Buschmann, M., Wang, D., Chaput, C., & Kandani, N. (2001). Rheological characterisation of
566 thermogelling chitosan/glycerol-phosphate solutions. *Carbohydrate Polymers*, *46*, 39–47.

567 Chenite, A., Chaput, C., Wang, D., Combes, C., Buschmann, M. D., Hoemann, C. D., … Selmani, A. (2000). Novel
568 injectable neutral solutions of chitosan form biodegradable gels in situ. *Biomaterials*, *21*(21), 2155–2161.
569 https://doi.org/10.1016/S0142-9612(00)00116-2

570 Cho, J., Heuzey, M. C., Bégin, A., & Carreau, P. J. (2005). Physical gelation of chitosan in the presence of β-
571 glycerophosphate: The effect of temperature. *Biomacromolecules*, *6*(6), 3267–3275.
572 https://doi.org/10.1021/bm050313s

573 Cho, J., Heuzey, M. C., Bégin, A., & Carreau, P. J. (2006). Effect of urea on solution behavior and heat-induced
574 gelationof chitosan-β-glycerophosphate. *Carbohydrate Polymers*, *63*(4), 507–518.
575 https://doi.org/10.1016/j.carbpol.2005.10.013

576 Crompton, K. E., Prankerd, R. J., Paganin, D. M., Scott, T. F., Horne, M. K., Finkelstein, D. I., … Forsythe, J. S.
577 (2006). Morphology and gelation of thermosensitive chitosan hydrogels. *Biophysical Chemistry*, *121*(1), 14–
578 20. https://doi.org/10.1016/j.bpc.2005.12.005

579 Custodio, C., Alves, C., Reis, R., & Mano, J. (2010). Immobilization of fibronectin in chitosan substrates improves
580 cell adhesion and proliferation. *Journal of Tissue Engineering and Regenerative Medicine*, (4), 316–323.
581 https://doi.org/10.1002/term

582 Deng, A., Kang, X., Zhang, J., Yang, Y., & Yang, S. (2017). Enhanced gelation of chitosan/β-sodium
583 glycerophosphate thermosensitive hydrogel with sodium bicarbonate and biocompatibility evaluated. *Materials*
584 *Science and Engineering C*, *78*, 1147–1154. https://doi.org/10.1016/j.msec.2017.04.109

585 Di Martino, A., Sittinger, M., & Risbud, M. V. (2005). Chitosan: A versatile biopolymer for orthopaedic tissue-
586 engineering. *Biomaterials*, *26*(30), 5983–5990. https://doi.org/10.1016/j.biomaterials.2005.03.016

587 Dmitrieva, N. I., & Burg, M. B. (2005). Hypertonic stress response. *Mutation Research - Fundamental and*
588 *Molecular Mechanisms of Mutagenesis*, *569*(1–2), 65–74. https://doi.org/10.1016/j.mrfmmm.2004.06.053

589 Filion, D., & Buschmann, M. D. (2013). Chitosan-glycerol-phosphate (GP) gels release freely diffusible GP and
590 possess titratable fixed charge. *Carbohydrate Polymers*, *98*(1), 813–819.
591 https://doi.org/10.1016/j.carbpol.2013.06.055

592 Filion, D., Lavertu, M., & Buschmann, M. D. (2013). Chitosan–glycerol-phosphate (GP) gels release freely
593 diffusible GP and possess titratable fixed charge. *Carbohydrate Polymers*, (98), 813–819.
594 https://doi.org/10.1016/j.carbpol.2013.06.055

595 Grinberg, V. Y., Burova, T. V., Grinberg, N. V., Tikhonov, V. E., Dubovik, A. S., Moskalets, A. P., & Khokhlov, A.
596 R. (2019). Thermodynamic insight into the thermoresponsive behavior of chitosan in aqueous solutions: A
597 differential scanning calorimetry study. *Carbohydrate Polymers*, *229*(September 2019), 115558.
598 https://doi.org/10.1016/j.carbpol.2019.115558

599 Huang, Z., Yu, B., Feng, Q., & Li, S. (2011). Modification of an injectable chitosan scaffold by blending with
600 NaHCO 3 to improve cytocompatibility. *Polymers and Polymer Composites*, *19*(9), 781–787.
601 https://doi.org/10.1177/096739111101900908

602 Huynh, N. C. N., Everts, V., Leethanakul, C., Pavasant, P., & Ampornaramveth, R. S. (2016). Rinsing with saline
603 promotes human gingival fibroblast wound healing in vitro. *PLoS ONE*, *11*(7), 1–13.
604 https://doi.org/10.1371/journal.pone.0159843

605 Kaivosoja, E., Barreto, G., Levón, K., Virtanen, S., Ainola, M., & Konttinen, Y. T. (2012). Chemical and physical
606 properties of regenerative medicine materials controlling stem cell fate. *Annals of Medicine*, *44*(7), 635–650.
607 https://doi.org/10.3109/07853890.2011.573805

608 Kondziolka, D., Gobbel, G. T., Fellows-Mayle, W., Chang, Y. F., & Uram, M. (2011). Injection parameters affect
609 cell viability and implant volumes in automated cell delivery for the brain. *Cell Transplantation*, *20*(11–12),
610 1901–1906. https://doi.org/10.3727/096368911X566190

611 Kornev, V. A., Grebenik, E. A., Solovieva, A. B., Dmitriev, R. I., & Timashev, P. S. (2018). Hydrogel-assisted
612 neuroregeneration approaches towards brain injury therapy: A state-of-the-art review. *Computational and*
613 *Structural Biotechnology Journal*, *16*, 488–502. https://doi.org/10.1016/j.csbj.2018.10.011

614 Kortum, G., Vogel, W., & Andrussow, K. (1960). Dissociation Constants of Organic Acids in Aqueous Solution. In
615 1961. London : Butterworths (Ed.), *Intern. union of pure and applied chemistry* (p. 241).

616 Lavertu, M., Filion, D., & Buschmann, M. D. (2008). Heat-induced transfer of protons from chitosan to glycerol
617 phosphate produces chitosan precipitation and gelation. *Biomacromolecules*, *9*(2), 640–650.
618 https://doi.org/10.1021/bm700745d

619 Li, C. H., & Tam, P. K. S. (1998). An iterative algorithm for minimum cross entropy thresholding. *Pattern*
620 *Recognition Letters*, *19*(8), 771–776. https://doi.org/10.1016/S0167-8655(98)00057-9

621 Li, X. Y., Kong, X. Y., Wang, X. H., Shi, S., Guo, G., Luo, F., … Qian, Z. Y. (2010). Gel-sol-gel thermo-gelation
622 behavior study of chitosan-inorganic phosphate solutions. *European Journal of Pharmaceutics and*
623 *Biopharmaceutics*, *75*(3), 388–392. https://doi.org/10.1016/j.ejpb.2010.04.015

624 Li, Y., Rodrigues, J., & Tomás, H. (2012). Injectable and biodegradable hydrogels: Gelation, biodegradation and
625 biomedical applications. *Chemical Society Reviews*, *41*(6), 2193–2221. https://doi.org/10.1039/c1cs15203c

626 Li, Z., Fan, Z., Xu, Y., Lo, W., Wang, X., Niu, H., … Guan, J. (2016). PH-Sensitive and Thermosensitive Hydrogels
627 as Stem-Cell Carriers for Cardiac Therapy. *ACS Applied Materials and Interfaces*, *8*(17), 10752–10760.

https://doi.org/10.1021/acsami.6b01374

Liu, L., Tang, X., Wang, Y., & Guo, S. (2011). Smart gelation of chitosan solution in the presence of NaHCO3for injectable drug delivery system. *International Journal of Pharmaceutics*, *414*(1–2), 6–15. https://doi.org/10.1016/j.ijpharm.2011.04.052

Mekhail, M., & Tabrizian, M. (2014). Injectable Chitosan-Based Scaffolds in Regenerative Medicine and their Clinical Translatability. *Advanced Healthcare Materials*, *3*(10), 1529–1545. https://doi.org/10.1002/adhm.201300586

Nair, L. S., Starnes, T., Ko, J. W. K., & Laurencin, C. T. (2007). Development of injectable thermogelling chitosan-inorganic phosphate solutions for biomedical applications. *Biomacromolecules*, *8*(12), 3779–3785. https://doi.org/10.1021/bm7006967

Neves, L. S., Babo, P. S., Gonçalves, A. I., Costa-Almeida, R., Caridade, S. G., Mano, J. F., … Gomes, M. E. (2017). Injectable Hyaluronic Acid Hydrogels Enriched with Platelet Lysate as a Cryostable Off-the-Shelf System for Cell-Based Therapies. *Regenerative Engineering and Translational Medicine*, *3*(2), 53–69. https://doi.org/10.1007/s40883-017-0029-8

O'Brien, F. J., Harley, B. A., Yannas, I. V., & Gibson, L. J. (2005). The effect of pore size on cell adhesion in collagen-GAG scaffolds. *Biomaterials*, *26*(4), 433–441. https://doi.org/10.1016/j.biomaterials.2004.02.052

Rinaudo, M. (2006). Chitin and chitosan: Properties and applications. *Progress in Polymer Science (Oxford)*, *31*(7), 603–632. https://doi.org/10.1016/j.progpolymsci.2006.06.001

Riva, R., Ragelle, H., Des Rieux, A., Duhem, N., Jérôme, C., & Préat, V. (2011). Chitosan and chitosan derivatives in drug delivery and tissue engineering. *Advances in Polymer Science*, *244*(1), 19–44. https://doi.org/10.1007/12_2011_137

Ruel-Gariépy, E., Chenite, A., Chaput, C., Guirguis, S., & Leroux, J. C. (2000). Characterization of thermosensitive chitosan gels for the sustained delivery of drugs. *International Journal of Pharmaceutics*, *203*(1–2), 89–98. https://doi.org/10.1016/S0378-5173(00)00428-2

San Juan, A., Montembault, A., Gillet, D., Say, J. P., Rouif, S., Bouet, T., … David, L. (2012). Degradation of chitosan-based materials after different sterilization treatments. *IOP Conference Series: Materials Science and Engineering*, *31*, 6–11. https://doi.org/10.1088/1757-899X/31/1/012007

Saravanan, S., Vimalraj, S., Thanikaivelan, P., Banudevi, S., & Manivasagam, G. (2019). A review on injectable chitosan/beta glycerophosphate hydrogels for bone tissue regeneration. *International Journal of Biological Macromolecules*, *121*, 38–54. https://doi.org/10.1016/j.ijbiomac.2018.10.014

Supper, S., Anton, N., Seidel, N., Riemenschnitter, M., Schoch, C., & Vandamme, T. (2013). Rheological study of chitosan/polyol-phosphate systems: Influence of the polyol part on the thermo-induced gelation mechanism. *Langmuir*, *29*(32), 10229–10237. https://doi.org/10.1021/la401993q

Ta, H. T., Han, H., Larson, I., Dass, C. R., & Dunstan, D. E. (2009). Chitosan-dibasic orthophosphate hydrogel: A potential drug delivery system. *International Journal of Pharmaceutics*, *371*(1–2), 134–141. https://doi.org/10.1016/j.ijpharm.2009.01.018

Tabet, A., Mommer, S., Vigil, J. A., Hallou, C., Bulstrode, H., & Scherman, O. A. (2019). Mechanical Characterization of Human Brain Tissue and Soft Dynamic Gels Exhibiting Electromechanical Neuro-Mimicry. *Advanced Healthcare Materials*, *8*(10), 1–5. https://doi.org/10.1002/adhm.201900068

Te Nijenhuis, K. (1979). *Dynamic mechanical studies on thermo-reversible ageing processes in gels of polyvinyl chloride and of gelatin*. Delf University.

Tsai, W. B., Chen, Y. R., & Liu, H. L. (2013). RGD-conjugated crosslinked chitosan scaffolds for culture and osteogenic differentiation of mesenchymal stem cells. *Journal of the Taiwan Institute of Chemical Engineers*, *44*(1), 1–7. https://doi.org/10.1016/j.jtice.2012.09.003

Wu, Y. S., van Vliet, L. J., Frijlink, H. W., & van der Voort Maarschalk, K. (2007). Pore size distribution in tablets measured with a morphological sieve. *International Journal of Pharmaceutics*, *342*(1–2), 176–183. https://doi.org/10.1016/j.ijpharm.2007.05.011

Yap, L. S., & Yang, M. C. (2020). Thermo-reversible injectable hydrogel composing of pluronic F127 and carboxymethyl hexanoyl chitosan for cell-encapsulation. *Colloids and Surfaces B: Biointerfaces*, *185*(September 2019), 110606. https://doi.org/10.1016/j.colsurfb.2019.110606

Zhang, H., Zhu, D., Song, L., Liu, L., Dong, X., Liu, Z., & Leng, X. (2011). Arginine conjugation affects the endocytic pathways of chitosan/DNA nanoparticles. *Journal of Biomedical Materials Research - Part A*, *98 A*(2), 296–302. https://doi.org/10.1002/jbm.a.33115

Zhou, H. Y., Jiang, L. J., Cao, P. P., Li, J. B., & Chen, X. G. (2015). Glycerophosphate-based chitosan thermosensitive hydrogels and their biomedical applications. *Carbohydrate Polymers*, *117*, 524–536. https://doi.org/10.1016/j.carbpol.2014.09.094